predict water concentrations in the solid residue closer to the lower end of the given range.
58. X. Xue, H. Baadsgaard, A. J. Irving, C. M. Scarfe, *J. Geophys. Res.* **95**, 15879 (1990).
59. D. A. Clague, W. S. Weber, J. E. Dixon, *Nature*, in press.
60. D. A. Clague and F. A. Frey, *J. Petrol.* **23**, 447 (1982).
61. D. A. Clague and J. E. Dixon, *Eos* 72, 563 (1991); J. E. Dixon, D. A. Clague, E. M. Stolper, in preparation.
62. A. E. Ringwood, *Phys. Earth Planet. Inter.* **3**, 109 (1970); C. R. Bina and B. J. Wood, *J. Geophys. Res.* **92**, 4853 (1987).
63. S. F. Foley, *Geochim. Cosmochim. Acta* **55**, 2689 (1991).
64. S. M. Peacock, *Science* **248**, 329 (1990).
65. A. W. Hoffman and W. M. White, *Earth Planet. Sci. Lett.* **57**, 421 (1982).
66. I. Kushiro, *J. Geophys. Res.* **95**, 15929 (1990).
67. M. O. Garcia, N. W. K. Liu, D. W. Muenow, *Geochim. Cosmochim. Acta* **43**, 305 (1979).
68. J. H. Davies and D. J. Stevenson, *J. Geophys. Res.*, in press.
69. H. P. Taylor, *J. Geol. Soc. London* **133**, 509 (1977).
70. J. Ingrin, K. Latrous, J. C. Doukhan, N. Doukhan, *Eur. J. Mineral.* **1**, 327 (1989).
71. E. Jagoutz *et al.*, *Proc. Lunar Planet. Sci. Conf.* **10**, 2031 (1979).
72. L. G. Liu, *Phys. Earth Planet. Inter.* **49**, 142 (1987).
73. L. W. Finger *et al.*, *Nature* **341**, 140 (1989).
74. T. Gasparik, *J. Geophys. Res.* **95**, 15751 (1990).
75. This research was supported by National Science Foundation grants EAR 88-16006 and EAR 91-04059. D.R.B. acknowledges financial support from the Harry Crossley Foundation and the American Federation of Mineralogical Societies. We thank our numerous sample donors, in particular J. J. Gurney, for their generosity, De Beers Consolidated Mines Ltd. for access to xenolith localities and collections, and G. S. Mattioli for help in the field. We are grateful to D. Endisch and F. Rauch at the University of Frankfurt for willingness to share unpublished nuclear reaction analysis data relevant to the calibrations used here. We have benefited from discussions with P. D. Ihinger, G. S. Mattioli, and E. M. Stolper, and we thank T. J. Ahrens, D. L. Anderson, J. E. Dixon, R. B. Hanson, P. J. Wyllie, and two anonymous reviewers for comments on drafts of this paper. This is Division of Geological and Planetary Sciences contribution no. 5071.

Direct Observation of Chemical Bond Dynamics on Surfaces

J. T. YATES, JR., M. D. ALVEY, M. J. DRESSER, M. A. HENDERSON, M. KISKINOVA, R. D. RAMSIER, A. SZABÓ

The dynamics of chemisorbed species as they swing to-and-fro on their adsorption sites may be directly observed with electron-stimulated desorption. The observation of the thermal disorder in adsorbate chemical bond directions, through studies of the thermal excitation of librational modes, allows one to visualize the potential energy surfaces controlling the structure and dynamics of adsorbates on single crystal metal and semiconductor surfaces. This information may be useful in understanding surface diffusion as well as the spatial aspects of surface chemical reactions.

THE BEHAVIOR OF THE CHEMICAL BONDS IN ADSORBED species is of central importance to all of surface chemistry. Indeed, the quest to understand chemical bonding at surfaces is one of the main driving forces in the field of surface science; much of current experimental and theoretical research is directed toward this general objective in one way or another. The understanding of surface bonding and reactivity has contributed immensely to the intellectual richness of the field of surface science. This knowledge has also had significant application to many diverse technologies that are controlled by surface phenomena. Among these are heterogeneous catalysis, semiconductor processing, corrosion prevention and other electrochemical technologies, many areas of materials science, and tribology.

The dynamics of molecules as they bond to a surface intimately influences the course of various thermally activated surface chemical phenomena. When a molecule interacts with a surface, the following sequence of dynamically governed events takes place: (i) adsorption from the gas; (ii) energy dissipation from the newly formed adsorbate; (iii) adsorbate libration, rotation, and vibration on its adsorption site; (iv) adsorbate diffusion with possible reaction at a neighbor site; and (v) desorption.

Modern experimental and theoretical methods of probing molecular dynamics have been applied to each of these categories of surface behavior, contributing both a classical (*1*) and a quantum mechanical (*2*) understanding of the elementary processes that determine the overall kinetics of chemical reactions on surfaces.

This article is concerned with the direct observation of the dynamics of chemisorbed species. It describes our current ability to observe the librations and rotations of chemisorbed species on their adsorption sites through the observation of the spatial patterns of thermal disorder induced in chemical bond directions. For research purposes, we select the symmetry and structure of the adsorption sites to be studied by using single crystal substrates that expose crystal planes of known structure. The substrate site structure controls the symmetry and shape of the potential energy surface that governs the motion of the thermally excited adsorbed molecules. These thermally activated motions probe the entry channels along the reaction coordinate that lead to surface diffusion and to surface reactions.

Adsorbed molecules, and also the atoms in the surface of a solid, may be studied in many ways with modern surface measurement techniques. Surface vibrational spectroscopy is one of the most powerful tools used to probe surface bonding (*3*). Information is sought about the vibrational modes and the forces coupling atoms and molecules on the surface. At the most primitive level of surface vibrational spectroscopy, observed frequencies of vibration are used as indicators of surface bond character through analogies to chemical group frequencies in molecules of known structure (*4*). More

---

J. T. Yates, Jr., and R. D. Ramsier are with the Surface Science Center, Department of Chemistry, University of Pittsburgh, Pittsburgh, PA 15260. M. D. Alvey is at 6385 Truman Street, Chino, CA 91710. M. J. Dresser is in the Department of Physics, Washington State University, Pullman, WA 99164. M. A. Henderson is with Battelle Northwest Laboratories, Post Office Box 999, Richland, WA 99357. M. Kiskinova is with Sincrotrone Trieste, Padiciano 99, 34012 Trieste, Italy. A. Szabó is in the Department of Chemistry, University of Washington, Seattle, WA 98195.

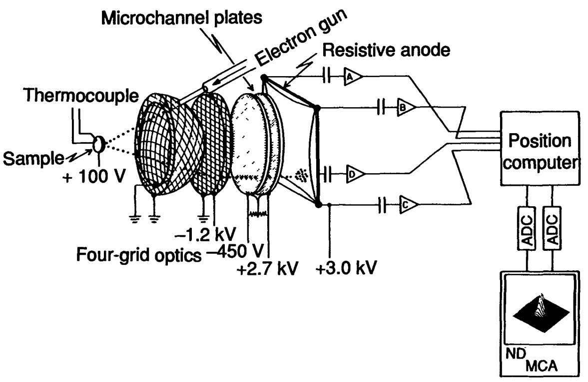

Fig. 1. Digital ESDIAD apparatus for measurement of angular distributions of species originating from electron-stimulated desorption from a single crystal surface. A distribution pattern is displayed on the MCA. ADC, analog-digital converter.

detailed interpretations consider intermolecular coupling phenomena between adsorbates as well as energy exchange between adsorbate and substrate (*5, 6*). Knowledge of dipole selection rules may often be used with the vibrational spectroscopies to obtain rough estimates of the surface bonding geometry of adsorbed species.

Electronic surface spectroscopies are also used as probes of surface bonding. Photoelectron spectroscopy (PES) probes the final state energies of holes in the valence band (ultraviolet excitation) or in atomic core levels (x-ray excitation) (7) and has been used for the study of the energy and occupancy of valence and core-level orbitals at the surface of both clean and adsorbate-covered solids. Angular resolved ultraviolet PES (ARUPS) can be used to determine bond orientations in chemisorbed species with an accuracy of ~10°. This accuracy, however, is insufficient to study the angular disorder in chemical bond directions due to thermal excitation. Angular resolved x-ray PES (ARXPS) has been used to measure adsorbate chemical bond directions with an accuracy of a few degrees (*8*), but the method is generally used in only one plane perpendicular to the surface and has not been used for adsorbate dynamics studies. Another useful technique, near-edge x-ray absorption fine structure (NEXAFS or XANES), can also be used to estimate chemical bond directions at surfaces (*9*). An accuracy of ~10° is the current limitation, also making this method inappropriate for bond dynamics studies.

One method, digital ESDIAD (electron-stimulated desorption ion angular distribution) (*10*), provides high precision (~1°) for measuring chemical bond directions, and hence bond dynamics, at surfaces. It relies on the electronic excitation of an oriented surface species by electron bombardment. The excited adsorbate ejects a molecular or atomic fragment (cation, anion, ground state, or electronically excited neutral) from the surface, along a direction nearly parallel to the direction of the bond being broken. These ejection directions are spatially imaged by single particle detection methods. Because the excitation and particle ejection processes are generally fast compared to the original nuclear motions in the adsorbate (rotation, libration, and vibration), ESDIAD effectively records a snapshot of the direction of the chemical bond being broken on a subpicosecond time scale for each molecule that produces a detectable particle. In a single experiment, ESDIAD can measure, as if superimposing many snapshots, the directions of millions of chemical bonds in an ensemble of adsorbed molecules on a single crystal as the molecules undergo their thermal motions. This composite ESDIAD image provides a statistical picture of the distribution of bond directions at a particular surface temperature. These images of the statistical distribution of the amplitudes of the low-frequency motions of adsorbed species provide a fascinating view of adsorbate dynamics not previously witnessed in such detail by other surface science measurement methods.

The ESDIAD Method—Its Discovery and How It Works

In 1974 it was found that simple adsorbed species on single crystal substrates could eject narrow beams of positive ions during electron-stimulated desorption (ESD) (*11*). The ion beams were often oriented in azimuthal directions corresponding to primary crystallographic directions on the substrate surface. It was postulated that the directionality of the sharp beams of ions was caused by the rupture of directional adsorbate-substrate bonds by ESD. Many studies involving the ESDIAD method have since been published, and a comprehensive review of ESD has recently appeared (*12*). Although the acronym ESDIAD was originally proposed for cases of positive ion production, it is now also used in cases producing negative ions or electronically excited neutrals. Many of the early ESDIAD studies involved the photographic imaging of the ion angular distribution; these studies were inherently unsatisfactory for fine-grained investigation of the detailed shapes of ESDIAD beams (needed for bond dynamics studies).

Such detailed ESDIAD studies are now possible by virtue of the better image quality associated with the single particle detection techniques of digital ESDIAD (*10*) (Fig. 1). The single crystal sample, containing adsorbed species, is exposed to a focused beam of electrons (1 mm^2) from the electron gun. Particles ejected from the surface by ESD, as well as backscattered primary and secondary electrons, encounter a four-grid electrostatic lens array. By proper grid biasing, positive and neutral species produced by ESD pass through the grid system, striking the first of two microchannel plate (MCP) amplifiers. Electron cascades that follow produce about 10^6 electrons in a pulse exiting the second MCP; this electron pulse is spatially coherent with each positive ion or electronically excited neutral species that hits the first MCP. This exiting electron pulse is accelerated into a resistive anode detector that determines the x and y coordinates of the pulse and, hence, the impact location on the first MCP of the single particle event causing the pulse. A statistical distribution of the particle arrival positions for millions of ESD events is accumulated in the multichannel analyzer (MCA), and a three-dimensional (3-D) digital ESDIAD pattern is produced. The stored pattern may be processed by smoothing routines (*13*), and the subtraction of a background due to a signal caused by soft x-rays may be made (*14*). One can separate positive ions produced by ESD from electronically excited neutral species by using a suitable positive grid bias on one of the internal grids. By reversing the grid potentials, one can use the apparatus for low-energy electron diffraction (LEED), giving information about the crystal surface structure. This information is needed to interpret the meaning of the angular patterns observed in ESDIAD.

Soon after the first ESDIAD measurements were reported, a number of theoretical models were advanced to explain the production of sharp ion beams in ESDIAD. Some of these models dealt with the repulsive potential experienced by the escaping positive ion (*15*); other models also considered initial-state effects associated with the adsorbate vibrational wave functions (*16*). In addition, both ion reneutralization and electrostatic image potential deflection of the escaping ions were quantitatively considered in the interpretation of ESDIAD patterns (*17–20*).

Despite the complexity and diversity of various theories, all models support the general principle that ESD induces a Franck-Condon excitation in a surface species from a vibrationally smeared ground state to a repulsive electronic state, which causes a particle to escape initially in a direction near the chemical bond direction. This process is illustrated in Fig. 2, where potential energy surfaces are schematically shown for the initial bond and for the ejected positive ion, A^+, from the ruptured bond. Indeed, this schematic multidimensional picture is derived from earlier one-dimensional models for ESD given independently by Menzel and Gomer (*21*) and by Redhead (*22*), now called the MGR model. Electronic excitation by photons to produce directed ion beams was subsequently demonstrated by Madey *et al.* (*23*) and interpreted with the same models used for ESDIAD. These models for ESD and ESDIAD, considered together with a wealth of experimental studies (*12*), leave little doubt that ESDIAD may be used to image bond directions in adsorbed species and that the dynamics associated with nuclear motions (or the dynamical motion of chemical bond directions) is contained in the ESDIAD beam shapes. Several examples are discussed below in which ESDIAD has provided an exciting view of the thermal disorder of the chemical bond directions in interesting adsorbates on metal and semiconductor crystal surfaces.

The Observation of the Rotation of an Adsorbed Molecule

Adsorbates of C_{3v} symmetry such as NH_3 and PF_3 have been extensively studied with ESDIAD and other techniques. These molecules offer the prospect, by virtue of surface bonding through the N or P atom to a surface atom, that they will project N–H or P–F bonds upward from the surface. ESDIAD imaging of these bond directions by observation of H^+ or F^+ ions would then yield the azimuthal orientation and the polar angle of the candidate bonds. In addition, molecules of this shape offer an opportunity to witness the thermal onset of molecular rotation about the vertical C_3 symmetry axis.

Such measurements for PF_3 adsorption on Ni(111) have in fact yielded the expected behavior (*24*). At low temperatures, PF_3 adsorbs as an azimuthally oriented molecule on top of Ni atom sites in the Ni(111) surface, which, at full coverage, form a p(2 × 2) overlayer (Fig. 3A). This overlayer consists of two domains that contain differently oriented PF_3 molecules and when considered together involve six P–F aximuthal bond orientations. Thus, a six-beam F^+ ESDIAD pattern is found, as shown schematically on the left-hand side of Fig. 3A. Whether the observed azimuthal orientations are due to intermolecular interactional effects at high coverage or to azimuthal adsorbate ordering by individual $PF_3 \cdots Ni(111)$ interactions was answered with ESDIAD studies at low PF_3 coverages, as shown on the left-hand side of Fig. 3B. At a surface coverage of $\theta_{PF_3} = 0.04$ PF_3/Ni, at which coverage PF_3 islands do not exist, a similar six-beam F^+ pattern is also seen. The P–F azimuths accurately orient along the six possible close-packed Ni–Ni directions on the crystal surface at 85 K. Chan and Hoffmann have theoretically deduced by using extended Hückel calculations that the atop-PF_3 site assignment and the observed azimuthal orientations shown here are energetically favored for a single PF_3 molecule on Ni(111) (*25*).

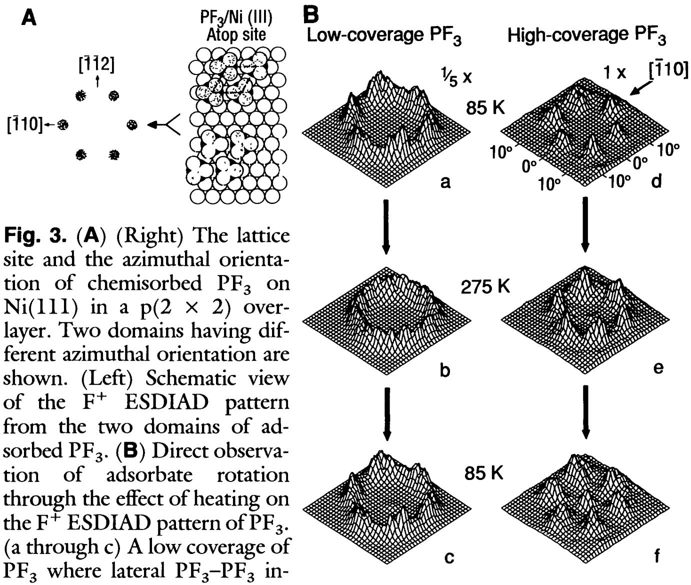

Fig. 3. (**A**) (Right) The lattice site and the azimuthal orientation of chemisorbed PF_3 on Ni(111) in a p(2 × 2) overlayer. Two domains having different azimuthal orientation are shown. (Left) Schematic view of the F^+ ESDIAD pattern from the two domains of adsorbed PF_3. (**B**) Direct observation of adsorbate rotation through the effect of heating on the F^+ ESDIAD pattern of PF_3. (a through c) A low coverage of PF_3 where lateral PF_3–PF_3 interactions are unimportant; (d through f) a high coverage of PF_3 where intermolecular interactions prevent PF_3 rotation. The central F^+ beam in (f) corresponds to a tiny fraction of PF caused by electron impact dissociation of PF_3.

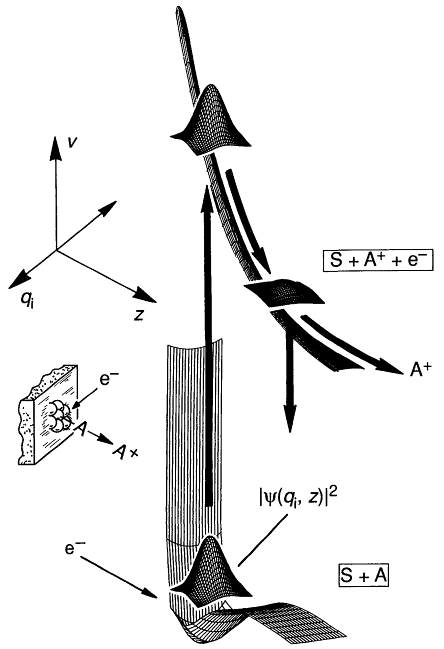

Fig. 2. Schematic potential energy surfaces for an adsorbed atom showing its excitation to a repulsive surface. Neutralization processes are effective in returning many A^+ ions to lower states. One of two generalized coordinates parallel to the surface is designated q_i. S, surface; A, adsorbate.

The dramatic effect of gently heating and cooling the surface is shown in Fig. 3B, a through c. At 275 K, essentially complete azimuthal disorder in the P–F bond directions is observed, producing a halo pattern from the six-beam F^+ pattern. Azimuthal reordering of the isolated PF_3 species occurs on cooling back to 85 K. Detailed quantitative studies of this temperature effect have yielded a rotational barrier height of 0.01 ± 0.002 eV (0.2 ± 0.05 kcal/mol) for isolated PF_3 molecules (*24*). At high coverages of PF_3, intermolecular effects between neighbor PF_3 molecules in p(2 × 2) islands (Fig. 3A) prevent molecular rotation (Fig. 3B, d through f). Heating the high-coverage layer to 275 K causes little azimuthal disorder, showing that molecular rotation is more strongly hindered at full coverage where p(2 × 2) PF_3 domains exist (Fig. 3B, d through f) (*24*). These studies led Zwanzig to consider statistical mechanical models for the rotation of interlocking surface rotors (*26*).

The isolated PF_3 molecule first begins to rotate about the Ni–P axis as thermal energy is absorbed. Little rocking of the C_3 axis away from the surface normal is observed at 275 K as the tiny "propeller" molecules spin on the surface. These experiments represent a direct nonspectroscopic observation of the excitation of the rotation of an adsorbate on a surface. The rotation of PF_3 on Ni(111) has also recently been observed to produce temperature-dependent infrared line shape changes (*27*). Isolated PF_3 molecules exhibit a small upward frequency shift of the symmetric PF_3 stretching mode upon rotational excitation.

Fig. 4. (**Right**) The lattice site and the azimuthal orientation of chemisorbed PF_2 and PF on Ni(111). These species are produced by electron impact dissociation of adsorbed PF_3. (**Left**) A schematic view of the F^+ ESDIAD pattern from a mixed layer of PF_2 and PF. Adsorbed F does not yield an appreciable F^+ signal.

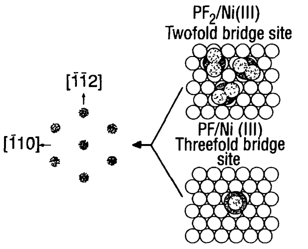

In contrast, ESDIAD studies of isolated PF_3 molecules on the hexagonally close-packed Ru(001) surface indicate that azimuthal rotation is not frozen out at 110 K, and only a F^+ halo is detected (*28*). Ammonia, a well-studied surface molecule, has never been frozen azimuthally on a metal surface; even at 29 K an H^+ halo is observed on Ni(110) (*29*). However, freezing of NH_3 rotation by lateral electrostatic interaction between NH_3 and other neighbor species has been observed in several ESDIAD studies (*30, 31*).

An interesting surface bonding effect that results from the removal of an H or an F atom from NH_3 or PF_3 has been observed by ESDIAD. NH_2 or PF_2 species, which are produced by relatively high levels of electron impact on their parent adsorbed molecules, are strongly bound and show new bond azimuths consistent with their individual mode of attachment to surface metal atoms (*32, 33*). For coordinatively unsaturated PF_2 (and PF), twofold and threefold Ni(111) adsorption sites, respectively, are selected as shown in Fig. 4. PF_2 and PF yield a new composite F^+ ESDIAD pattern compared to PF_3 in Fig. 3, A and B. These new bonding sites for chemisorbed PF_2 and PF are theoretically predicted to be the stable surface sites on Ni(111) (*25*). Similar experimental results have also been obtained for PF_2 and PF on Ru(001) (*28*). On the basis of these ideas, we have demonstrated that electron impact methods can be used to produce high surface coverages of unusual surface species such as NH_2 or NH (*32, 33*). These species are postulated to be the chemical intermediates in the NH_3 synthesis on heterogeneous catalysts (*34*). This electron impact–induced synthetic route to adsorbed catalytic intermediates therefore provides the surface scientist with an unusual opportunity to examine the properties of these important surface species in detail through the use of the many surface analytical probes currently available.

Dynamic and Static Tilting of Adsorbates

Studies of the chemisorption of diatomic molecules such as CO or NO have provided new insights into the factors that may influence the librational amplitude and the average tilt directions of these molecules. Madey studied the librational motions of adsorbed CO using an apertured mass spectrometer for ion detection (*35*). For CO bound to atop sites on Ru(001), normally directed CO^+ and O^+ beams broadened as the surface temperature was increased from 90 to 300 K. Menzel *et al.* (*36*) showed that a slight broadening of CO^+ and O^+ ESDIAD beams occurs as the CO coverage on Ru(001) is increased, which was interpreted as indicating an increase of interadsorbate repulsions that caused the CO molecule to statically tilt an average of 5° from the surface normal at saturation coverage.

New insights into CO libration and static tilting have been provided from studies of CO chemisorbed on Pt surfaces (*37*). In this case, in addition to ESD-induced CO^+ and O^+ ion production, copious yields of a metastable electronically excited species ($a^3\pi$-CO, called CO*) are observed. CO* is believed to be formed through a direct electronic excitation, not from CO^+ reneutralization (*37*). Most importantly, CO* trajectories are not significantly altered by electrostatic image effects from the substrate because CO* is a neutral species experiencing only weak dipole-image effects as it leaves the metal surface. Thus, the angular distribution of CO* closely matches the Pt–CO bond directions. The thermal broadening of the CO*, O^+, and CO^+ ESDIAD beams are shown in Fig. 5A at θ_{CO} = 0.50 CO/Pt (*37*). The widths of the three beams increase significantly because of the thermal excitation of CO librations, and a detailed calculation of the contribution of bond tilting to this broadening effect has recently been made (*38*).

In the coverage regime above θ_{CO} = 0.50 CO/Pt, static tilting of chemisorbed CO occurs in particular surface directions because of increased CO intermolecular repulsions as the coverage is increased. The ESDIAD behavior of the CO^+ ion angular distribution in the high-coverage regime above θ_{CO} = 0.50 is shown in Fig. 5B. The

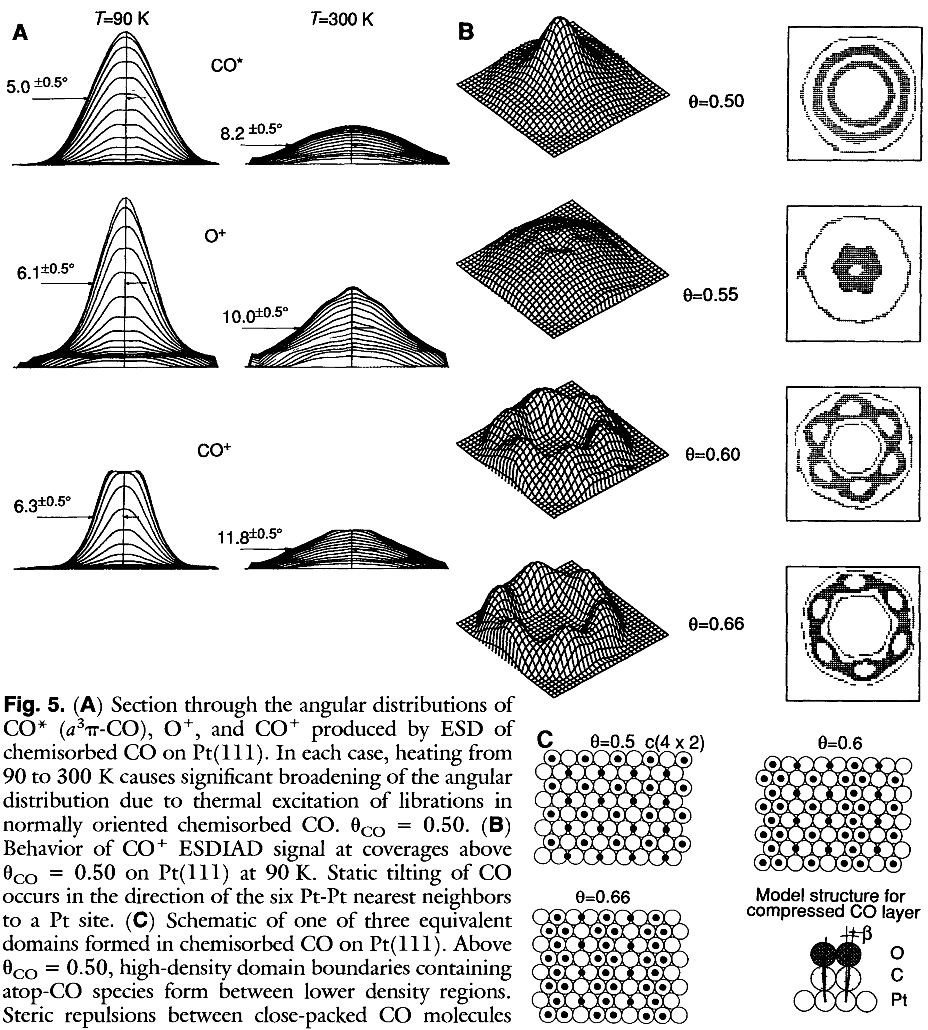

Fig. 5. (**A**) Section through the angular distributions of CO* ($a^3\pi$-CO), O^+, and CO^+ produced by ESD of chemisorbed CO on Pt(111). In each case, heating from 90 to 300 K causes significant broadening of the angular distribution due to thermal excitation of librations in normally oriented chemisorbed CO. θ_{CO} = 0.50. (**B**) Behavior of CO^+ ESDIAD signal at coverages above θ_{CO} = 0.50 on Pt(111) at 90 K. Static tilting of CO occurs in the direction of the six Pt-Pt nearest neighbors to a Pt site. (**C**) Schematic of one of three equivalent domains formed in chemisorbed CO on Pt(111). Above θ_{CO} = 0.50, high-density domain boundaries containing atop-CO species form between lower density regions. Steric repulsions between close-packed CO molecules produce a tilt angle away from the normal (β = 6°), leading to the CO^+ patterns shown in (B).

CO$^+$ beams tilt away from the normal in six directions that correspond to the Pt–Pt nearest neighbor directions in the substrate surface plane. This is caused by triple domain formation of closely packed atop-CO species. One of the three domains is shown in Fig. 5C; somewhat similar structures involving slightly higher CO coverages are reported by Persson *et al.* (*39*). Studies of CO* angles with ESDIAD reveal a Pt–CO tilt angle (β) of 6° as shown schematically in the lower right-hand corner of Fig. 5C.

This work forms the basis for answering the important question of whether foreign atoms coadsorbed with CO influence the CO librational dynamics. In fact, both S and Se, at a coverage of $\theta = 0.25$, cause a significant sharpening of the CO* ESDIAD beams, which occurs because of repulsive steric effects between librating CO molecules and the adsorbed chalcogenide atoms. These effects may be related to catalytic poisoning; the poisons (S and Se) may limit the dynamical motions of the CO molecule, and hence the chemical reactivity (*40*). Electronic effects are also certainly involved in catalytic poisoning (*41*).

Dynamics of Molecules Adsorbed on Defect Sites

The use of single crystal substrates for studies of adsorbed species offers a rich opportunity to examine the molecular behavior of adsorbates on defect sites. Step defect sites, arranged in a periodic order, may be produced by cutting single crystals at known angles slightly inclined from the low index planes (*42*). Upon cleaning and annealing of the atomic-stepped crystals, one uses LEED to verify that surface reconstruction of the stepped surface has not occurred, and one may then proceed to study adsorbed species on the defect step sites. Atomic step sites often act as traps for mobile adsorbed species (*43–45*). In this case, one can deliver molecules specifically to the atomic step sites, keeping the terrace sites free of adsorbed species (*46*). By careful control, the coverage of CO, present exclusively on the parallel linear chains of step sites, may be adjusted at will. Assuming there are no interactions between molecules on neighboring steps, this permits the observation of independent linear arrays of adsorbed species; that is, one can see the detailed behavior of one-dimensional chemisorbed layers.

Two schematic drawings of the {112} plane of Pt are shown in Fig. 6A. The plane consists of three-atom-wide terraces of Pt(111) microfacets separated by one-atom-high steps of Pt(001) orientation. The ESDIAD detector can be aligned perpendicular to the macroscopic normal to the crystal as shown in View 1. In View 2 the detector is rotated 20° in the downstairs direction. These two detector orientations permit the observation of step and terrace CO bonding angles over their full range. The variety of Pt–CO bonding angles observed as the CO coverage is increased from 0.19 CO/Pt to 0.79 CO/Pt is shown in Fig. 6B. The CO* images are shown, which avoid image charge distortions of the trajectories of the escaping particles. In View 2 (which images molecules on the step sites), initially, the only CO* beam is a single beam that is oriented in a direction −20° from the normal to the macroscopic plane. This indicates that the adsorbed CO molecules on the step sites are inclined by about 20° in the downstairs direction. As the coverage increases, this beam is attenuated, and CO* beams inclined left and right by ±13° appear. At still higher CO coverages, the left and right beams are extinguished, and two beams at 0° and −38° develop, indicating tilt directions orthogonal to those observed at intermediate coverages. View 1 is arranged for the observation of CO molecules originating mainly from the terrace sites. At high coverages, a beam of CO* at +13° is characteristic of CO molecules tilting upstairs on the terrace sites, probably on Pt atoms directly adjacent to the step atoms.

A model showing the structures proposed on the step sites (viewed by looking upstairs on the stepped crystal) is given in Fig. 6C. At an average coverage of $\bar{\theta} = 0.19$ monolayer (ML), a (2 × *n*) unit cell is observed with LEED; this is due to a population of only a single type of CO species inclined −20° in the downstairs direction on the step sites. Here the step sites are one-half filled. As the steps fill to three-quarters coverage, corresponding to $\bar{\theta} = 0.24$ ML, "triplets of CO" are formed, exhibiting CO* beams in three directions as CO molecules adjacent to the central molecule are inclined over empty sites in directions parallel to the steps, producing the beams at ±13°. When the steps are completely filled ($\bar{\theta} > 0.56$), a new set of CO tilt directions upstairs and downstairs is established. Development of a CO* beam originating from the terraces can first be observed at a coverage of $\bar{\theta} = 0.34$ ML, as shown in View 1 of Fig. 6B. This +13° angle of inclination from the normal to the Pt(112) macroscopic plane indicates that CO molecules on the terrace sites are inclined upstairs from the step sites containing adsorbed CO species.

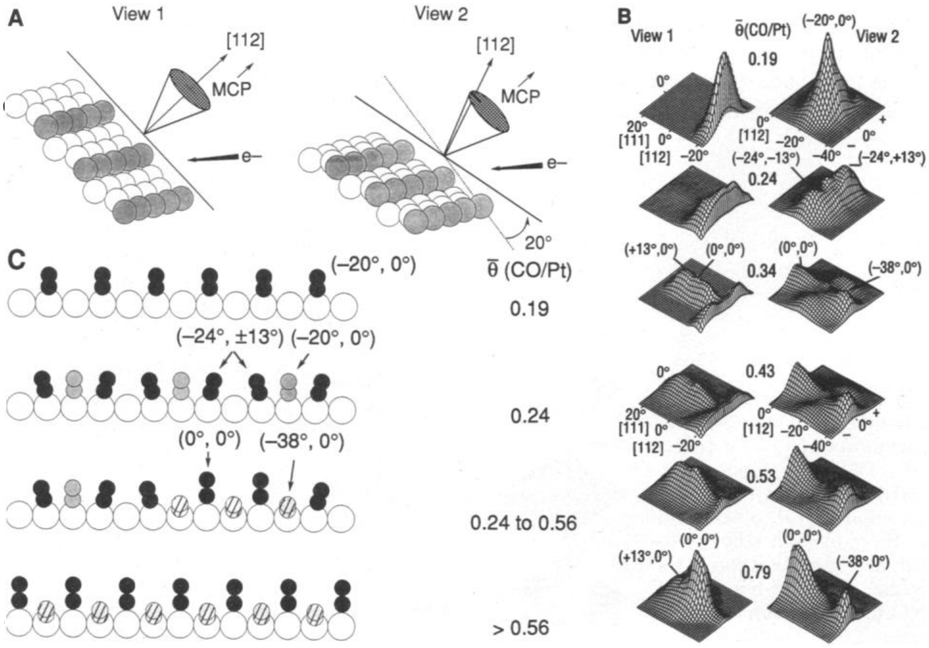

Fig. 6. (**A**) Schematic view of the Pt(112) stepped surface. The ESDIAD detector sees either View 1 (MCP parallel to the crystal face and normal to [112]) for studies of adsorbed CO species on the terrace sites, or View 2 (crystal face rotated 20° away from the analyzer axis) for studies of these species on the step sites. (**B**) Direct observation of Pt–CO bond directions with ESDIAD studies of the CO* angular distributions. View 1 mainly shows CO on the terraces; View 2 mainly shows CO on the steps. As the CO coverage is increased, the step sites are filled first and exhibit orthogonal CO tilt directions with increasing CO coverage as shown in View 2. (**C**) Proposed structures of CO on the step sites on Pt(112). Tilt angles are in parentheses: (down the step, along the step). The steps are viewed from downstairs as the CO coverage is increased.

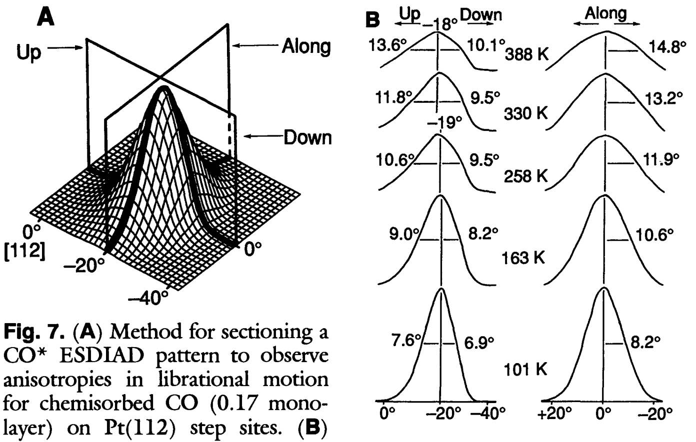

Fig. 7. (**A**) Method for sectioning a CO* ESDIAD pattern to observe anisotropies in librational motion for chemisorbed CO (0.17 monolayer) on Pt(112) step sites. (**B**) Cross sections of CO* ESDIAD patterns for increasing temperature for chemisorbed CO (0.06 monolayer) on step sites of Pt(112). The asymmetry in the up-down sections reflects the details of the interaction of the CO molecule with the Pt sites in its vicinity.

The repulsions between CO molecules causing the tilting in various directions are an example of steric effects where overlapping electron clouds on adjacent molecules cause the repulsions. Calculations of the magnitude of the electrostatic repulsive energy due to dipole-dipole repulsions between adjacent CO molecules show that this repulsive energy is far too small to explain the angles observed experimentally (*47*). This experiment, involving linear arrays of chemisorbed molecules at low coverages, is an intriguing illustration of the intricate bonding behavior that may be observed in fine detail with the ESDIAD method.

The high-resolution capability of ESDIAD has been further exploited in experiments designed to measure the thermally excited dynamics of CO adsorbed on the Pt step defect sites (*46*). For this purpose, CO adsorbed only in the downstairs tilted structure at low coverages on Pt(112) step sites was used. At the step sites the potential energy surfaces that govern the librational amplitudes of chemisorbed CO species are asymmetrical. Figure 7A illustrates how a CO* ESDIAD pattern from CO on the step site is analyzed in order to observe anisotropies in the librational motion. The measured pattern is sliced cross sectionally by planes perpendicular and parallel to the step edge direction. The cross sections of the ESDIAD patterns increase in width as the temperature is raised, indicating that thermal excitations are being observed (Fig. 7B). The cross-sectional profiles in the "up-down" direction are asymmetrical; the larger half-width is in the upstairs direction. The profiles in the "along" direction are symmetrical, as would be expected, because any step adsorption site is symmetrical in its relation to neighboring Pt atoms along the step.

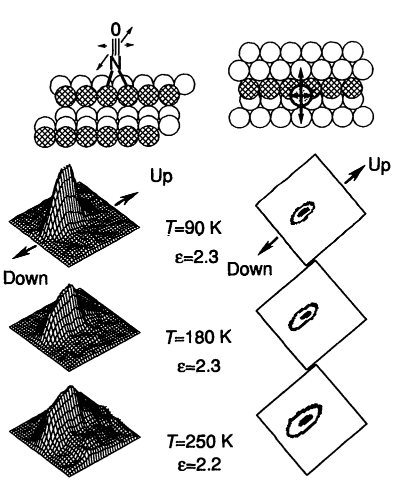

Fig. 8. Strong asymmetries in librational amplitudes of chemisorbed NO on step sites of Pt(112) (from O^+ ESDIAD patterns). The largest amplitudes are observed in a direction perpendicular to the step-edge direction. This is due to bridge-bonding of NO to two Pt atoms on the step.

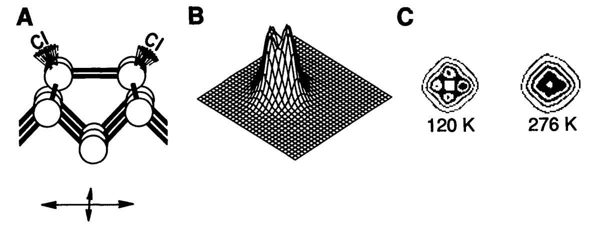

Fig. 9. Dynamics of Si–Cl bonds. (**A**) Symmetric dimer site in a single domain on Si(100) that contains Si–Cl surface groups. Librational motion of the Cl atom is schematically indicated; arrows indicate orthogonal domain directions. (**B**) Four-beam Cl^+ ESDIAD pattern from the superposition of two orthogonal classes of Si dimer domains on Si(100) at 120 K. (**C**) Contour diagrams of Cl^+ ESDIAD patterns at two temperatures. The (reversible) thermal broadening of the four Cl^+ beams into a distorted halo pattern is clearly seen. The F^+ patterns have been compressed toward the normal by electrostatic means.

One can interpret these results by considering the frustrated translational modes of chemisorbed CO. These large-amplitude modes have a librational frequency with energy of about 0.006 eV (*48*). The largest librational amplitudes are observed with ESDIAD in the "along" direction and indicate that at low coverages, the CO molecules have the softest frustrated translational modes in a direction parallel to the step edges. The smallest librational amplitudes are observed in the "downstairs" direction and may reflect the repulsive interaction of the orbital electron cloud of the inclined CO molecule with electron density that has spilled out onto the terrace from the step site (*49, 50*). The high degree of freedom of frustrated translational vibrations parallel to the step edge may be an indication of the most favorable surface migration direction available to CO on the defect surface (*46*), but this hypothesis remains to be confirmed by other methods.

Another interesting investigation of a diatomic molecule's interaction with the stepped Pt(112) surface is shown in Fig. 8. The result offers insight into the use of the ESDIAD method to observe adsorbate dynamics and to observe the state of hybridization of adsorbates on their adsorption sites. At low coverages, NO forms a bridged bond with two Pt atoms on various Pt surfaces (*51–54*). This type of bonding at a step site would be expected to produce anisotropic frustrated translational motions, in which higher amplitude librations occur in the direction perpendicular to the plane of the adsorbed molecule compared to the in-plane direction. These expectations follow from cluster calculations of Richardson and Bradshaw (*55*). For the sp^2-hybridized molecule bridge-bonded to two Pt step atoms, the direction of largest librational amplitude should be perpendicular to the step edge direction.

Digital ESDIAD measurements (*56*) of this system have been carried out, yielding the expected result shown in Fig. 8. In this study, the O^+ species was analyzed, and a highly anisotropic ESDIAD pattern was observed. Cross sections through the pattern show an ellipticity of about 2.3. The long axis of the ellipse is aligned perpendicular to the step edge. The angular width of the pattern in both directions increases as the temperature is increased, indicating that thermally excited molecular librations in chemisorbed NO are being observed. Control experiments showed that anisotropic electrostatic image effects on O^+ ions could not produce the elliptical O^+ patterns observed from NO (*56*). Thus, ESDIAD was able to confirm, through observation of librational dynamics alone, that NO is bridge-bonded to step Pt sites.

Application of ESDIAD to Adsorbates on Covalent Solid Surfaces

The application of ESDIAD to the study of adsorbates on semiconductor surfaces is just beginning. Understanding adsorbate bonding and dynamics on semiconductor surfaces is of great importance because of the technological need to control chemical processing methods for electronic device fabrication. Semiconductors, in contrast to metals, are internally bonded by directed covalent bonds, and unsatisfied valencies (dangling bonds) project upward from the surface. It is here that adsorbates form highly localized chemical bonds to the surface. The first ESDIAD studies on a covalent surface, Si(100), concerned the adsorption of fluorine (*57*). More recently, –Cl groups produced by Cl_2 chemisorption on Si(100)-(2 × 1) have been investigated with ESDIAD (*58*). A four-beam Cl^+ pattern is observed at low temperatures as shown in Fig. 9, B and C. These Cl^+ beams originate from Si–Cl covalent bonds, which are inclined from the surface normal in four specific directions at an angle of ~30° from the surface normal. These four directions correspond to the orthogonal Si–Si surface dimer bond directions exposed on alternate terraces of Si(100); the steps and terraces are caused by slight misalignment of the crystal, and a symmetric dimer site in one domain is shown in Fig. 9A. Recent NEXAFS measurements report the Si–Cl bond to be normal to the Si(100)-(2 × 1) surface, but the accuracy of these measurements is only ±10° (*59*).

With gentle heating, the Si–Cl bond directions become significantly broadened as a result of the excitation of librational modes. This effect may easily be seen by comparison of Cl^+ ESDIAD contour patterns obtained at two temperatures (Fig. 9C). Thermal broadening of the Cl^+ beams results in the conversion of the sharp four-beam pattern into a pattern with Cl^+ intensity in certain regions between the four beams, yielding a Cl^+ ESDIAD pattern resembling a distorted halo. Figure 9A shows one possible site structure (a symmetric Si dimer) containing adsorbed Cl species that undergo thermal disordering of the Si–Cl bond directions at elevated temperatures. Recent high-resolution XPS studies of Si(100) (2 × 1) have shown that the clean surface consists of asymmetric Si_2 dimers having rather large differences in electronic charge on the two Si atoms constituting the dimer site (*60*).

Future Directions

The ESDIAD technique is often useful for imaging the chemical bond directions in adsorbates and also in imaging the thermal disorder that occurs in these bond directions. ESDIAD gives a detailed view of the motional freedom of adsorbed species on adsorption sites of known structure. Such information cannot be obtained at present even from atomic resolution techniques such as the scanning tunneling microscope (STM), the atomic force microscope (AFM), or the field ion microscope (FIM). If the mode of highest amplitude, as imaged with ESDIAD, corresponds to the preferred reaction coordinate for surface diffusion or surface reaction, then ESDIAD potentially provides a way to spatially image the onset of activated diffusion or the spatial character of reaction processes on surfaces. This important and far-reaching hypothesis must be tested in the future for validity and generality.

The current and future application of existing and new experimental methods to probe the dynamics of desorbing species produced by electronic excitation offers many rich opportunities for understanding adsorbate potential surfaces, surface photochemistry, and surface thermochemistry at a deeper level. The molecular- and atomic-level concepts derived from this information should prove useful in advancing our ability to understand and control major technological areas dominated by surface chemistry.

REFERENCES AND NOTES

1. J. C. Tully, in *Many Body Phenomena at Surfaces*, D. Langreth and H. Suhl, Eds. (Academic Press, Orlando, FL, 1984) pp. 377–401; J. W. Gadzuk, *Annu. Rev. Phys. Chem.* **39**, 395 (1988).
2. A. E. Depristo and A. Kara, *Adv. Chem. Phys.* **77**, 163 (1990).
3. J. T. Yates, Jr., and T. E. Madey, Eds., *Vibrational Spectroscopy of Molecules on Surfaces* (Plenum, New York, 1987).
4. M. R. Albert and J. T. Yates, Jr., *The Surface Scientist's Guide to Organometallic Chemistry* (American Chemical Society, Washington, DC, 1987), p. 3.
5. F. M. Hoffmann, *Surf. Sci. Rep.* **3**, 107 (1983); Y. J. Chabal, *ibid.* **8**, 211 (1988).
6. E. Schweizer, B. N. J. Persson, M. Tüshaus, D. Hoge, A. M. Bradshaw, *Surf. Sci.* **213**, 49 (1989).
7. G. Ertl and J. Küppers, *Low Energy Electrons and Surface Chemistry* (VCH, Weinheim, Federal Republic of Germany, 1985), pp. 65–146.
8. D. A. Wesner, F. P. Coenen, H. P. Bonzel, *Phys. Rev. B* **39**, 10770 (1989).
9. D. C. Koningsberger and R. Prins, *Principles, Applications and Techniques of EXAFS, SEXAFS and XANES* (Wiley, New York, 1988).
10. J. T. Yates, Jr., M. D. Alvey, K. W. Kolasinski, M. J. Dresser, *Nucl. Instrum. Methods Phys. Res. B* **27**, 147 (1987).
11. J. J. Czyzewski, T. E. Madey, J. T. Yates, Jr., *Phys. Rev. Lett.* **32**, 777 (1974).
12. R. D. Ramsier and J. T. Yates, Jr., *Surf. Sci. Rep.* **12** (6–8), 243 (1991); see also T. E. Madey, *Science* **234**, 316 (1986).
13. A. Szabó, M. Kiskinova, J. T. Yates, Jr., *Surf. Sci.* **205**, 207 (1988).
14. M. J. Dresser, M. D. Alvey, J. T. Yates, Jr., *ibid.* **169**, 91 (1986).
15. J. I. Gersten, R. Janow, N. Tzoar, *Phys. Rev. Lett.* **36**, 610 (1976).
16. W. L. Clinton, *ibid.* **39**, 965 (1977).
17. ______, *Surf. Sci.* **112**, L791 (1981).
18. D. P. Woodruff, *ibid.* **124**, 320 (1983).
19. T. E. Madey, in *Inelastic Particle-Surface Collisions*, vol. 17 of *Springer Series in Chemical Physics*, E. Taglauer and W. Heiland, Eds. (Springer, Berlin, 1981), pp. 80–103.
20. Z. Mišković, J. Vukanić, T. E. Madey, *Surf. Sci.* **141**, 285 (1984); *ibid.* **169**, 405 (1986).
21. D. Menzel and R. Gomer, *J. Chem. Phys.* **40**, 1164 (1964); *ibid.* **41**, 3311 (1964).
22. P. A. Redhead, *Can. J. Phys.* **42**, 886 (1964).
23. T. E. Madey, R. Stockbauer, J. F. van der Veen, D. E. Eastman, *Phys. Rev. Lett.* **45**, 187 (1980).
24. M. D. Alvey, J. T. Yates, Jr., K. J. Uram, *J. Chem. Phys.* **87**, 7221 (1987).
25. A. W. E. Chan and R. Hoffmann, *ibid.* **92**, 699 (1990).
26. R. Zwanzig, *ibid.* **87**, 4870 (1987).
27. X. Guo, J. T. Yates, Jr., V. K. Agrawal, M. Trenary, *ibid.* **94**, 6256 (1991).
28. T. E. Madey, S. A. Joyce, A. L. Johnson, J. A. Yarmoff, in *Desorption Induced by Electronic Transitions, DIET IV*, G. Betz and P. Varga, Eds. (Springer-Verlag, Berlin, 1990), pp. 176–181, and references therein.
29. C. Klauber, M. D. Alvey, J. T. Yates, Jr., *Chem. Phys. Lett.* **106**, 477 (1984).
30. T. E. Madey and C. Benndorf, *Surf. Sci.* **152/153**, 587 (1985); F. P. Netzer and T. E. Madey, *Phys. Rev. Lett.* **47**, 928 (1981).
31. M. J. Dresser, A.-M. Lanzillotto, M. D. Alvey, J. T. Yates, Jr., *Surf. Sci.* **191**, 1 (1987).
32. C. Klauber, M. D. Alvey, J. T. Yates, Jr., *ibid.* **154**, 139 (1985); see also I. C. Bassignana, K. Wagemann, J. Küppers, G. Ertl, *ibid.* **175**, 22 (1986).
33. M. D. Alvey and J. T. Yates, Jr., *J. Am. Chem. Soc.* **110**, 1782 (1988).
34. G. Ertl, *Crit. Rev. Solid State Mater. Sci.* **10**, 349 (1982); J. K. Norskov and P. Stoltze, *Surf. Sci.* **189/190**, 91 (1987).
35. T. E. Madey, *Surf. Sci.* **79**, 575 (1979).
36. W. Riedl and D. Menzel, *ibid.* **163**, 39 (1985); *ibid.* **207**, 494 (1989).
37. M. Kiskinova, A. Szabó, A.-M. Lonzillotto, J. T. Yates, Jr., *ibid.* **202**, L559 (1988).
38. A. Szabó and J. T. Yates, Jr., unpublished results.
39. B. N. J. Persson, M. Tüshaus, A. M. Bradshaw, *J. Chem. Phys.* **92**, 5034 (1990).
40. M. Kiskinova, A. Szabó, J. T. Yates, Jr., *ibid.* **89**, 7599 (1988); *Phys. Rev. Lett.* **61**, 2875 (1988).
41. M. Kiskinova, *Surf. Sci. Rep.* **8**, 359 (1988).
42. G. A. Somorjai, *Chemistry in Two Dimensions* (Cornell Univ. Press, Ithaca, NY, 1981), pp. 156–168.
43. B. Poelsema, R. L. Palmer, G. Comsa, *Surf. Sci.* **123**, 152 (1982).
44. J. E. Reutt-Robey, D. J. Doren, Y. J. Chabal, S. B. Christman, *Phys. Rev. Lett.* **61**, 2778 (1988).
45. H. R. Siddiqui, P. J. Chen, X. Guo, J. T. Yates, Jr., *J. Chem. Phys.* **92**, 7690 (1990).
46. M. A. Henderson, A. Szabó, J. T. Yates, Jr., *ibid.* **91**, 7245 (1989); *ibid.*, p. 7255.
47. ______, *Chem. Phys. Lett.* **168**, 51 (1990).
48. A. M. Lahee, J. P. Toennies, Ch. Wöll, *Surf. Sci.* **177**, 371 (1986).
49. R. Smoluchowski, *Phys. Rev.* **60**, 661 (1941).
50. J. Tersoff and L. M. Falikov, *Phys. Rev. B* **24**, 754 (1981).
51. B. E. Hayden, *Surf. Sci.* **131**, 419 (1983).
52. J. L. Gland and B. A. Sexton, *ibid.* **94**, 355 (1980).
53. H. Ibach and S. Lehwald, *ibid.* **76**, 1 (1978).
54. R. J. Gorte and J. L. Gland, *ibid.* **102**, 348 (1981).
55. N. V. Richardson and A. M. Bradshaw, *ibid.* **88**, 255 (1979).
56. A. Szabó, M. A. Henderson, J. T. Yates, Jr., *J. Chem. Phys.* **92**, 2208 (1990).
57. M. J. Bozack, M. J. Dresser, W. J. Choyke, P. A. Taylor, J. T. Yates, Jr., *Surf. Sci.* **184**, L332 (1987); see also A. L. Johnson, M. M. Walczak, T. E. Madey, *Langmuir* **4**, 277 (1988).
58. C. C. Cheng, Q. Gao, J. T. Yates, Jr., in preparation; Q. Gao, C. C. Cheng, J. T. Yates, Jr., in preparation.
59. D. Purdie *et al.*, in preparation.
60. G. K. Wertheim, D. M. Riffe, J. E. Rowe, P. H. Citrin, *Phys. Rev. Lett.* **67**, 120 (1991).

61. We thank the Air Force Office of Scientific Research for support.